

On the corotation torque for low-mass eccentric planets

Stephen M. Fendyke^{*} and Richard P. Nelson

Astronomy Unit, School of Physics and Astronomy, Queen Mary, University of London, United Kingdom

Accepted 2013 September 30. Received 2013 September 30; in original form 2013 July 12

ABSTRACT

We present the results of high resolution 2D simulations of low mass planets on fixed eccentric orbits embedded in protoplanetary discs. The aim of this study is to determine how the strength of the sustained, non-linear corotation torque experienced by embedded planets varies as a function of orbital eccentricity, disc parameters, and planetary mass. In agreement with previous work we find that the corotation torque diminishes as orbital eccentricity, e , increases. Analysis of the time-averaged streamlines in the disc demonstrates that the width of the horseshoe region narrows as the eccentricity increases, and we suggest that this narrowing largely explains the observed decrease in the corotation torque. We employ three distinct methods for estimating the strength of the unsaturated corotation torque from our simulations, and provide an empirical fit to these results. We find that a simple model where the corotation torque, Γ_C , decreases exponentially with increasing eccentricity (i.e. $\Gamma_C \propto \exp(-e/e_f)$) provides a good global fit to the data with an e-folding eccentricity, e_f , that scales linearly with the disc scale height at the planet location. We confirm that this model provides a good fit for planet masses of 5 and 10 M_\oplus in our simulations. The formation of planetary systems is likely to involve significant planet-planet interactions that will excite eccentric orbits, and this is likely to influence disc-driven planetary migration through modification of the corotation torque. Our results suggest that high fidelity models of planetary formation should account for these effects.

Key words:

1 INTRODUCTION

The current dataset describing the observed population of extrasolar planets displays a broad diversity in physical and orbital properties. Inspection of the currently confirmed exoplanets¹ (Wright et al. 2011) reveals the existence of numerous short-period massive planets (‘hot-Jupiters’), and multiple planet systems composed of compact, short-period bodies of low and intermediate mass (super-Earths and Neptune-like planets). Examples of these latter systems include Kepler-11 with six planets (Lissauer et al. 2011), Kepler-20 with five (Gautier III et al. 2012), Kepler-62 with five (Borucki et al. 2013) and HD 10180 with up to seven detected by the HARPS spectrograph (Lovis et al. 2011). Numerous other multi-planet systems have also been reported in the literature (Endl et al. 2012; Fabrycky et al. 2012; Lissauer et al. 2012; S. Udry et al. 2007). Taken as a whole, these planetary systems are likely to contain substantial mass in heavy elements, such that their existence is difficult to explain using *in situ* formation scenarios because

most disc models contain insufficient inventories of solid material at small radii (e.g. Hayashi 1981; Weidenschilling 1977). Large scale migration, possibly coupled with continuing mass growth, would appear to provide the most compelling explanation for many of these systems, although N-body models coupled with disc-driven migration have so far not managed to reproduce short-period multi-planet systems that are particularly similar to those observed (e.g. McNeil & Nelson 2010).

While planet-planet gravitational scattering coupled with tidal interaction with the central star may explain some short-period planets, the compact, low mutual-inclination, short-period systems such as Kepler-11 appear to be best explained through gas disc-driven migration. Low mass planets whose Hill radii are smaller than the local scale height (such that they do not carve out deep, tidally-truncated gaps) experience type I migration, driven by a combination of Lindblad and corotation torques (Goldreich & Tremaine 1980; Ward 1997; Tanaka et al. 2002). Particular interest has focussed on the role of corotation torques since it was first realised that they may counterbalance the rapid inward migration driven by Lindblad torques. In particular, strong positive gradients in disc surface density can cause

^{*} E-mail: S.M.Fendyke@qmul.ac.uk

¹ see <http://exoplanets.org>

the corotation torque to stall migration due to the associated gradient in vortensity (Masset et al. 2006), and a negative entropy gradient may also cause migration to stall (Paardekooper & Mellema 2006; Baruteau & Masset 2008; Paardekooper & Papaloizou 2008).

Strong corotation torques (also known as “horseshoe drag” (Ward 1991)) arise through interaction between the planet and gas that executes horseshoe orbits in a disc with a radial gradient in vortensity and/or entropy. Given that horseshoe streamlines are a non-linear phenomenon, horseshoe drag is also referred to as the non-linear corotation torque (Paardekooper & Papaloizou 2008). The vortensity-related corotation torque is prone to saturation in the absence of viscosity, which maintains the vortensity gradient across the horseshoe region against the tendency of orbital phase mixing there to flatten it out. Similarly, thermal diffusion or cooling is required to maintain the entropy-related corotation torque against saturation. Torque formulae have been derived that allow the steady-state corotation torque to be calculated for a broad range of disc and planet parameters (Paardekooper et al. 2010, 2011; Masset & Casoli 2010).

In addition to saturation in the absence of viscous or thermal diffusion, the corotation torque has been shown to diminish if the planet orbit becomes eccentric (Bitsch & Kley 2010). At present the physical reason for this decrease is not clear, and as yet there has not been an extensive analysis of how the dependence of the corotation torque on eccentricity scales with variations in disc and planet parameters. Given that planet-planet interactions during planet formation and migration lead inevitably to eccentricity excitation (e.g. Cresswell & Nelson 2006), further exploration of these issues is important in order to fully understand the role of migration in planetary formation. Using simple N-body simulations of planetary accretion coupled with prescriptions for type I migration torques obtained from Paardekooper et al. (2011), Hellary & Nelson (2012) examined the possible influence of eccentricity excitation on the oligarchic growth of planets, and concluded that the ability of horseshoe drag to prevent rapid inward migration of growing planets is diminished strongly when the associated quenching of the corotation torque is accounted for. Further examination of this is clearly required to test the assumptions of how the torque scales with eccentricity adopted in this latter study.

In this paper, we present results from 2D hydrodynamic simulations of eccentric planets of different mass embedded in protoplanetary discs with differing effective vertical scale heights. Particular challenges faced when analysing the results include the tendency for moderate gaps and vortices to form in low viscosity discs with relatively small vertical scale heights (i.e. $H/r \lesssim 0.05$). To overcome these problems three different methods for estimating the unsaturated corotation torque were employed. As expected from the earlier simulations of Bitsch & Kley (2010), we observe that the corotation torque decreases as the planet eccentricity increases. We provide an empirically derived analytic fit formula for our simulation results which shows that the corotation torque decreases exponentially with orbital eccentricity, with the e-folding eccentricity scaling linearly with the local disc scale height.

The paper is organised as follows: In section 2 we dis-

cuss our methodology and simulation setup. In section 3 we present the simulation results, and in section 4 we discuss and interpret these results. We draw our conclusions in section 5.

2 METHODOLOGY

2.1 Disc model

To compute the disc model, we use a modified version of the magnetohydrodynamic code NIRVANA (Ziegler 1998), which is based on the ZEUS algorithm (Stone & Norman 1992), to solve the vertically integrated hydrodynamic equations in polar coordinates (R, ϕ) :

$$\partial_t \sigma + \nabla \cdot (\sigma \vec{v}) = 0 \quad (1)$$

$$\partial_t (\sigma \vec{v}) + \nabla \cdot [\sigma \vec{v} \vec{v}] = -\nabla P - \sigma \nabla \Phi \quad (2)$$

$$\partial_t e + \nabla \cdot (e \vec{v}) = -P \nabla \cdot \vec{v} + \mathcal{Q} - \Lambda \quad (3)$$

where e is the internal energy density, \mathcal{Q} and Λ are heating and cooling terms, v is velocity, P is pressure, σ is the surface density and Φ is the combined gravitational potential of the central star and the planet. We use an ideal gas equation of state to close the system of equations: $P = (\gamma - 1)e$ with the adiabatic exponent $\gamma = 1.4$.

We simulate an embedded planet in a non self-gravitating two-dimensional disc with inner and outer radii located at 0.5 and 1.8 au, respectively. Reflecting boundary conditions are employed at the radial boundaries, in conjunction with damping zones that minimise wave reflection using the scheme presented in Val-Borro et al. (2006). We use a resolution of either 1020 or 1024 cells in radius and 2048 in azimuth. The simulations are computed in a frame corotating with the guiding centre of the planet, such that the eccentricity is manifest as epicyclic motion around this guiding centre. The gravitational force of the planet acting on the disc is softened using a softening parameter, $b = 0.4h$. The disc density profile takes the form $\sigma = \sigma_0 r^{-\alpha}$ with $\alpha = 0.5$, and the temperature profile is $T = T_0 r^{-\beta}$ with $\beta = 2.0$. Our disc mass is normalised by $\sigma_0 = 1.35 \times 10^{-3}$.

We consider planets with mass ratios $q = 1.5 \times 10^{-5}$ and 3×10^{-5} (equivalent to 5 and 10 Earth mass planets orbiting a solar-type star). The orbit remains fixed, and is integrated using a fifth order Runge-Kutta scheme, while the torque experienced by the planet is recorded as a time series.

As described in the introduction, preventing saturation of the entropy related corotation torque requires thermal diffusion of the gas so that the entropy gradient across the horseshoe region is maintained. Rather than including a computationally expensive full-blown radiative transfer model, we have implemented a simple Newtonian cooling scheme that constantly forces the entropy in the disc back toward its initial value on a specified time scale, τ_{ent} . The value of τ_{ent} is chosen through experiment to optimally unsaturate the corotation torque. Given that P/σ^γ is a constant along each adiabat and is therefore a function of entropy, s , we define the function

$$K(s) = \frac{P}{\sigma^\gamma}, \quad (4)$$

and iterate it at each timestep according to

$$K_{i+1}(s) = K_i(s) - (K_i(s) - K(s_0)) \frac{\Delta t}{\tau_{ent}}, \quad (5)$$

where $K(s_0)$ is the initial value of the entropy function and Δt is the time-step size. From this, the internal energy density is recalculated using the ideal gas law

$$e = K(s) \frac{\sigma^\gamma}{\gamma - 1}. \quad (6)$$

2.2 Simulations

We computed disc models with aspect ratios $h \equiv H/r = 0.03, 0.05, 0.07$ and 0.1 . For each value of h , eccentricity values in the interval $0 \leq e \leq 0.3$ were considered. For each combination of h and e , we performed two separate simulations:

(A) An adiabatic disc with viscosity at the lowest value consistent with obtaining a well-behaved time series for the measured torque on the planet. We give these values in table 1. In the absence of this small viscosity we find that torque time series may become difficult to interpret due to strong time-dependencies introduced through the development of small vortices that form near the separatrices between circulating and librating material. A low viscosity adiabatic disc allows saturation of both the vortensity and entropy related contributions to the corotation torque as material in the horseshoe region becomes phase mixed and the vortensity and entropy gradients disappear. A torque time series from one of these simulations when the planet is on a circular orbit is shown in figure 1.

(B) A disc with viscosity and thermal diffusion set to values selected by successive trials to optimally unsaturate the corotation torque. We give the optimal values in table 1. The torque time series from such a simulation with a circular orbit is shown in figure 1. We note that all torques plotted in this paper are normalised by the quantity Γ_0/γ where

$$\Gamma_0 = \left(\frac{q}{h}\right)^2 \sigma_p r_p^4 \Omega_p^2, \quad (7)$$

and q is the planet-star mass ratio m_p/M_* , r_p is the planet orbital radius, and Ω is the Keplerian angular velocity. A subscript ‘p’ denotes evaluation at the planet location.

For all simulations, as the non-linear horseshoe drag is due to material undergoing horseshoe orbits, and the timescale for even the shortest horseshoe orbit is significantly longer than the planetary orbital period, we continually construct and record time-averaged density and velocity fields from the disc for further analysis. We also maintain a record of the contribution to the torque exerted on the planet by the disc as a function of radius in the disc.

For simulations in set A, it is assumed that after the total torque has reached a steady-state, the corotation torque has saturated and only the Lindblad torque remains. For those in set B, we expect the steady-state total torque to approach the value predicted by the formulae of Paardekooper et al. (2010) for unsaturated corotation torques in the circular orbit case. Using these two sets of simulations, we estimate the corotation torque for each different eccentricity using three methods:

(i) By taking the difference between the long-term, steady-state, time-averaged torques obtained in the corresponding

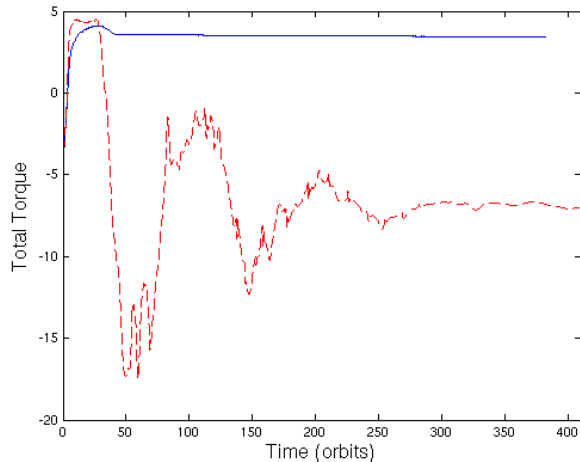


Figure 1. Torque time series for a disc with optimally unsaturated corotation torque (blue, solid line) and saturated torque (red, dotted line) respectively. Time is given in orbits and torque is shown in units of Γ_0/γ . In both simulations, the disc thickness is $H/r = 0.05$ and the planet is fixed on a circular orbit.

Table 1. Optimised entropy relaxation timescale, τ_{ent} , optimised kinematic viscosity, ν_{opt} , and minimum kinematic viscosity, ν_{min} , that allows for a quasi-steady flow for a planet on a circular orbit in a disc of various thicknesses. These values are obtained through numerical experimentation.

H/r	τ_{ent} (orbits)	ν_{opt}	ν_{min}
0.03	7	8×10^{-6}	2.5×10^{-7}
0.05	11	5×10^{-6}	1×10^{-7}
0.07	13	4×10^{-6}	1×10^{-7}
0.10	14	1.5×10^{-6}	1×10^{-8}

simulations from sets A and B. This method assumes that the Lindblad torque is the same in each simulation, such that the torque difference measures the unsaturated corotation torque obtained in the set B simulation directly.

(ii) By using time-averaged velocity fields to determine the extent of the region in which disc material is undergoing horseshoe orbits. We aggregate the torque contribution from this region by using time-averages of the torque versus radius data that we accumulate during the simulations.

(iii) By measuring the initial peak in the torque time series from simulations in set A associated with the initial growth of the corotation torque prior to its long-term saturation. This is the method most similar to previous measurements of the corotation torque (Paardekooper et al. 2010). The peak is then compared with the long-term steady torque which is assumed to comprise the Lindblad torque only due to saturation of the corotation torque.

2.3 Torque filtering

The torque time series for an eccentric planet consists of an average value, due to the motion of the planet’s guiding centre, and a contribution due to the epicyclic motion that varies quasi-periodically on the planet orbital period. At

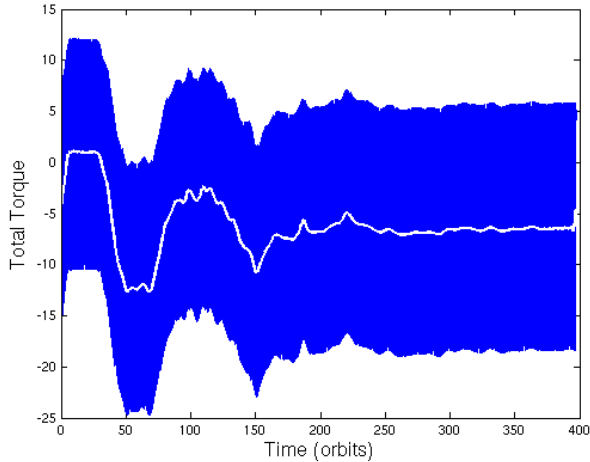


Figure 2. A torque time series for a planet with eccentricity, $e = 0.02$ in a disc with $h = 0.05$ (blue). Superimposed is the same time series with the high frequency oscillations in torque due to the planet’s epicyclic motion filtered out (white).

high eccentricities, the contribution from the epicyclic motion dominates and obscures the averaged value that we require. As this motion occurs on a much more rapid timescale than that of material within the corotation region, we use a Fourier transform filter to remove oscillations occurring on timescales more rapid than a few orbital periods. The result of employing this procedure is shown in figure 2.

3 RESULTS

In this section we present the results from the simulations. We show time-averaged surface density fields for a sample of the runs in which sustained, unsaturated corotation torques were obtained, and the magnitudes of corotation torques estimated using the three methods described in section 2.2. For each set of corotation torque results we obtain a simple analytical fit that describes the variation of corotation torque with eccentricity.

In figure 3 we show time-averaged steady-state surface density fields for the $h = 0.07$ discs with optimised, sustained corotation torques. Using the corresponding time-averaged velocity fields, we locate and superimpose the circulating streamline that sits closest to the horseshoe region (interior and exterior to the planet) where the gas is seen to librate rather than circulate. As such, this streamline acts as the boundary that separates the circulating and librating regions. Inspection of figure 3 shows clearly the tendency for the width of the horseshoe region to decrease as the eccentricity increases, with the horseshoe streamline u-turns broadly confined to the region outside the path of the planet’s epicyclic motion. Furthermore, each panel shows the presence of a positive surface density perturbation within the horseshoe region that sits just ahead of the planet, and a negative perturbation that sits just behind it (in the inertial frame, the sense of motion in this figure would be from left to right). As has been discussed in previous work (e.g. Baruteau & Masset 2008), these perturbations arise from the advection of fluid elements on horseshoe orbits that

almost conserve their entropy (and vortensity) around the horseshoe u-turn (in the absence of viscosity, thermal relaxation or shocks these quantities should be conserved). Maintenance of local pressure equilibrium causes regions that receive low entropy material from the outer disc to contract. Regions behind the planet that receive high entropy material expand. The resulting surface density perturbations lead to the observed positive corotation torque, as shown earlier in figure 1, for example. This perturbation is present in all simulations presented in figure 3, but diminishes as the eccentricity increases and the width of the horseshoe region decreases because the advected entropy introduces a reduced pressure perturbation.

Each of the panels in figure 3 shows the characteristic spiral density wave, but as the eccentricity increases the single wave that is present interior and exterior to the planet splits into two well-defined wake-like structures. This arises because the epicyclic motion of the planet around its guiding centre causes the planet to travel more slowly than local disc material when at apocentre, and faster than local material when at pericentre. This leads to periodic excitation of inward and outward propagating wakes at these two phases of the orbit, as described for example in Kley & Nelson (2012)². The relative motion between gas and planet at apocentre and pericentre also leads to a reversal of the normally negative Lindblad torque when $e \geq h$. This is because orbiting gas is gravitationally focussed to a region that leads the planet at apocentre, creating a positive density perturbation in front of the planet that exerts a positive torque. This provides the dominant contribution to the orbit-averaged torque because the planet spends most of its time at apocentre. This reversal of the Lindblad torque for $e > h$ was first reported by Papaloizou & Larwood (2002), who presented torque calculations based on summing contributions from numerous eccentric Lindblad resonances.

We now present results on how the corotation torque varies with eccentricity and disc parameters, showing the results obtained with each of the methods used to estimate the corotation torque. We begin by presenting results for planet mass $5 M_{\oplus}$ and disc models with $h = 0.03, 0.05$ and 0.07 , followed by a model with $5 M_{\oplus}$ and $h = 0.1$. Finally, we present a model with planet mass $10 M_{\oplus}$ and $h = 0.1$.

3.1 Method (i): Comparing torque time series

When using this method to estimate the steady corotation torque as a function of eccentricity, we first filter out high frequency oscillations in the torque time-series due to the epicyclic motion of the planet, and then take the difference between the results of simulations in sets A and B. In principle, the long-term steady torques in set A converge to pure Lindblad torques, and those in set B consist of the Lindblad plus sustained corotation torque, so we take the difference and use this as a measure of the corotation torque. The results obtained using this method are shown in figure 4, where we plot the estimated corotation torque value versus

² An animation associated with this review article, showing the influence of a $30 M_{\oplus}$ planet on an eccentric orbit with $e = 0.1$ embedded in a disc with $H/r = 0.05$, may be seen at <http://www.youtube.com/watch?v=65nqq9sEZdM>

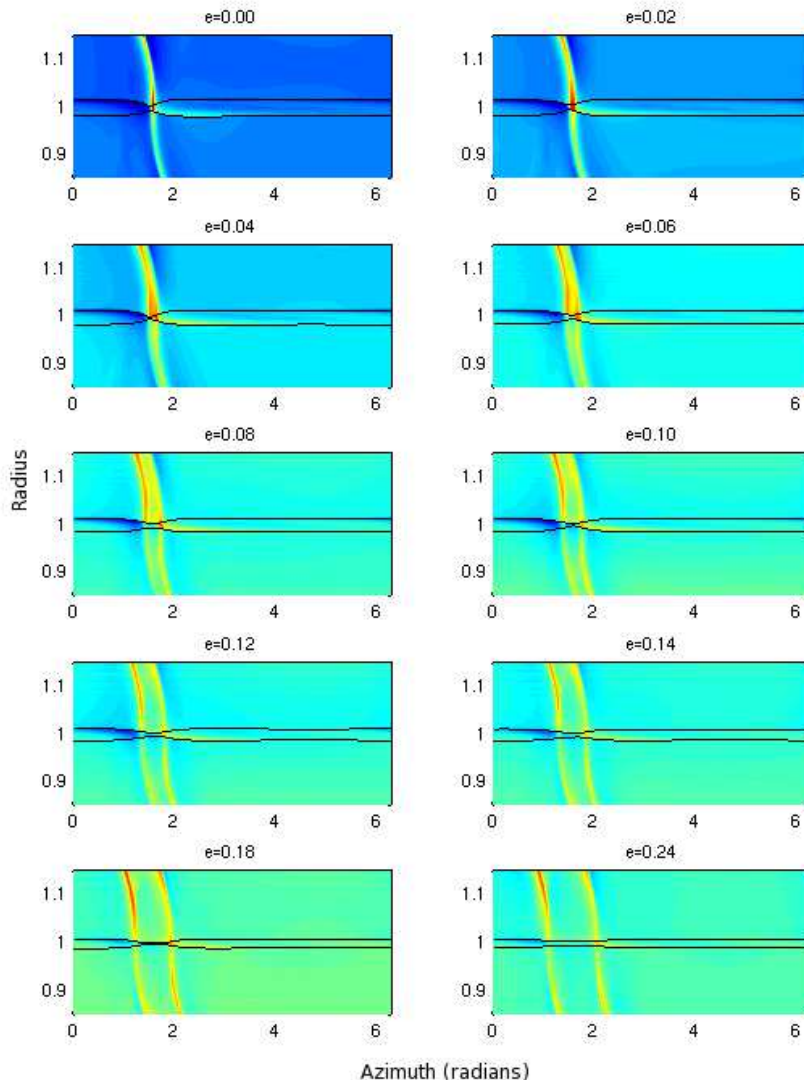


Figure 3. The time-averaged fractional perturbation of the initial disc surface density, with the last circulating streamline superimposed. Fields are plotted between 0.85 and 1.1 orbital radii of the planet and for the entire azimuth of the disc, for eccentricities between 0 and 0.24. The colours used are not to the same scale. The disc used to generate these fields has aspect ratio, $h = 0.07$. Note (i) the narrowed horseshoe region for increased eccentricities, which we associate with decreased corotation torque; (ii) the ‘splitting’ of the distinctive spiral density wave into two strands at increased eccentricity; and (iii) the presence of a sustained density perturbation within the corotation region (between the last circulating streamlines).

eccentricity. As there is residual time variation in the torque at the end of the simulations, we plot the mean torque (averaged between 240 and 350 orbits), and error bars showing three standard deviations about the mean.

The simulations from set B with thermal relaxation and viscosity produce smooth, well-behaved results that tend toward a well-defined steady state after sufficient run-time. There are a number of issues, however, affecting some low-viscosity disc models from set A that combine to make it difficult to obtain accurate estimates of corotation torques.

They involve restructuring of the disc in some fashion. First, we find that the thinner, low viscosity disc models develop moderate gaps due to tidal torques from the planet. These have depth $\sim 10\text{-}20\%$ of the background surface density. Although these models do not satisfy the usual gap formation requirement that the planet Hill sphere size exceeds the vertical scale height (see e.g. Lin & Papaloizou 1993; Crida et al. 2006), non-linear damping of the spiral waves deposits angular momentum in the disc near the planet and can cause a moderate annular dip to develop in the local

surface density profile. This effect has been predicted analytically by Rafikov (2002) and observed in simulations by Muto et al. (2010). The gap impacts on the estimate of the Lindblad torque in these cases, and therefore affects the corotation torque estimate because a similar gap does not develop in the corresponding viscous disc model.

The second issue is that for eccentricities $e \geq 0.06$ in the $h = 0.03$ runs, a large scale discrete vortex forms very close to the corotation radius of the planet guiding centre. This moves very slowly relative to the planet, but exerts a time-varying torque on it that is very difficult to average out because of the long run times that would be required. This clearly has an effect on our ability to measure the corotation torque using method (i). Finally, for some runs with $h = 0.03$ and 0.05 , and for intermediate values of the eccentricity (i.e. $0.07 \lesssim e \lesssim 0.1$), we observe the development of discrete structures in the simulations. When the time averaged surface density is rendered using contour plots similar to those shown in figure 1 we observe these structures to sit in or at the inner edge of the horseshoe region close to the mean location of the planet. They do not appear to be vortices, but instead seem to be features related to the high density structure that forms behind the planet at pericentre. As can be seen in the middle panel of figure 4, for example, this is an issue that affects the torque for the $e = 0.08$ and 0.1 cases for this particular value of h . So far we have been unable to determine why only these specific runs give rise to this phenomenon.

In figure 5, we show the total torques as a function of eccentricity from all our simulations with planet mass $5 M_{\oplus}$ and $h = 0.03, 0.05$ and 0.07 . These are the torques used by method (i) to calculate the corotation torque, and are particularly of note because they display the total torque (including the unsaturated corotation torque) and the Lindblad torque. In agreement with Papaloizou & Larwood (2002), the Lindblad torque changes sign from negative to positive values for $e > 1.1h$, and we see that at large values of e the two sets of torque values essentially coincide as the corotation contribution diminishes.

3.2 Method (ii): Streamline-defined horseshoe region

This method estimates the corotation torque by defining a region of the disc to be the horseshoe region through inspection of fluid streamlines obtained from time averages of the disc velocity field taken over many orbits of the planet. A starting location is chosen in the disc from which we construct fluid streamlines by integrating the averaged velocity field. Bilinear interpolation is used to define the local velocity away from the centres of grid cells. By performing this integration for a large number of closely separated initial locations, we are able to precisely locate the region in which material undergoes horseshoe turns on average. In our parlance, the location between librating and circulating material is delineated by the ‘last circulating streamline’. There is one interior and exterior to the planet’s semi-major axis. In figure 6 we plot half the distance between the inner and outer last circulating streamlines as a function of azimuth for all models drawn from set B that we are considering in this section ($m_p = 5 M_{\oplus}$ and $h = 0.03, 0.05, 0.07$). Each line corresponds to a simulation with different planet eccentric-

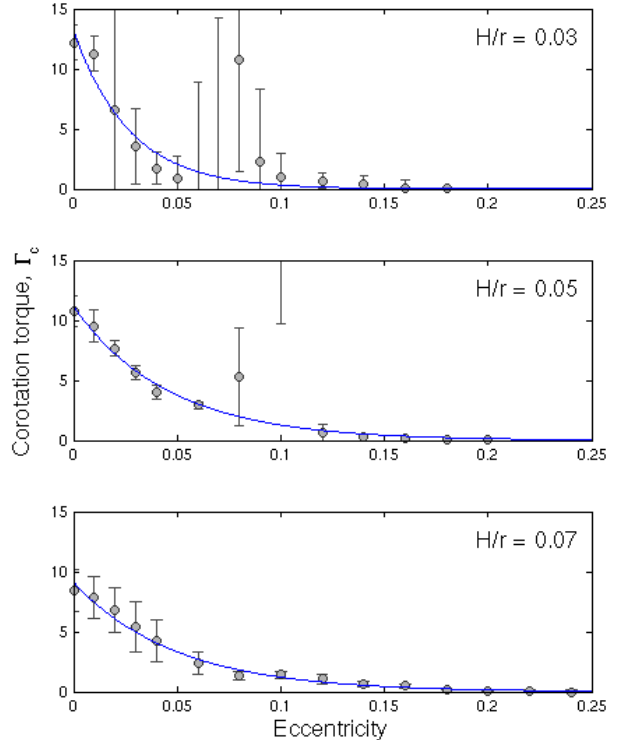


Figure 4. We plot the corotation torque measured by method (i); by taking the difference in steady state total torque between simulations with a saturated and optimally unsaturated corotation torque (sets B and A respectively). High-frequency oscillation in the torque due to the epicyclic motion of the planet has been filtered out, and the error bars shown are three times the combined standard deviations of the mean steady state torques. Results are given for three disc aspect ratios and fits are of the form $\Gamma_c = \Gamma_{c,e=0} \exp\left(-\frac{e}{e_f}\right)$. Corotation torque is given in units of Γ_0/γ .

ity, and we note the clear trend for the horseshoe region to narrow as e increases. The half-width of the corotation region is smallest for the most eccentric planets in the thickest disc, where $x_s \sim 0.01$, and we note that this is resolved by ~ 10 cells in our simulations. We remind the reader that for the $h = 0.07$ disc, these streamlines are also shown in figure 3. We have noted previously that they narrow for increasing eccentricity, and that the density perturbations associated with the corotation torque are contained within the defined boundaries of the corotation region.

For the purpose of calculating the corotation torque using method (ii), the corotation region is taken to be an annulus whose width is defined to be the distance between the points on the inner and outer last circulating streamlines that are furthest from the planet’s orbital radius. Once the corotation region has been defined, the gravitational force exerted by disc material on the planet from within that region is summed and time-averaged. Given that we are interested in measuring the steady corotation torque we apply this method to simulations in set B only. In general we expect the corotation torques to be localised within this horse-

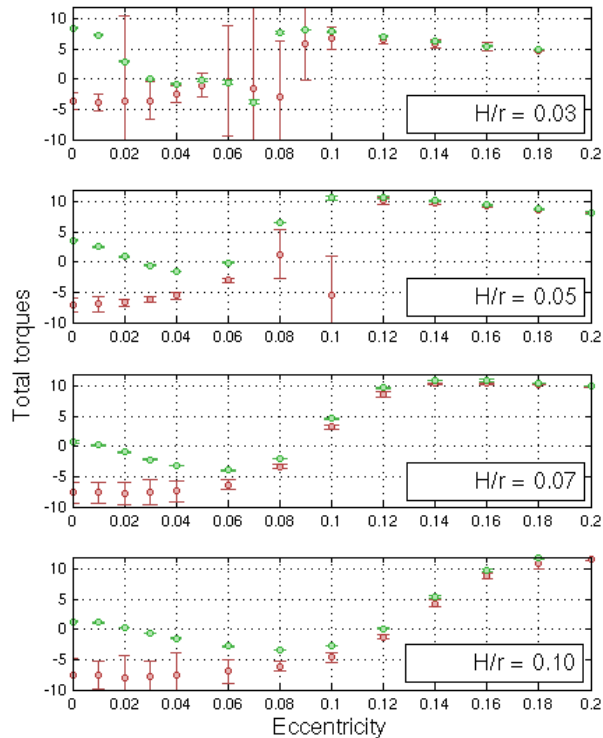


Figure 5. Total torque as a function of eccentricity for simulations from set A (green) and set B (red). Note the transition in torque from negative to positive values at around $1.1h$.

shoe region, and the Lindblad torque to originate from beyond a distance to the planet equal to $2H/3$. In figure 7, we show the torque acting on the planet as a function of radius in the disc, demonstrating the localisation of the two torque contributions to these regions. Further features displayed in the figure are worthy of note. We see the magnitude of the corotation torque decrease with increasing eccentricity, and we also observe the Lindblad torque contributions from the inner and outer disc change sign as the eccentricity exceeds h . Furthermore, for the higher eccentricity cases we see the contributions from the inner and outer disc torques originate from the pericentre and apocentre of the planet orbit.

The estimates of the steady corotation torques for each of the models with planet mass equal to $5 M_{\oplus}$ and $h = 0.03, 0.05$ and 0.07 are shown in figure 8. The filled circles represent values for the corotation torque obtained by taking a fiducial value for the width of the horseshoe region (the distance between the points on the inner and outer last circulating streamlines that are furthest from the planet’s orbital radius). The error bars represent the fact that there is some ambiguity in the corotation torque because the last circulating streamlines used to define the boundary of the corotation region do not lie at constant distance from the corotation radius of the planet guiding centre. These error bars were obtained by moving the boundary of the corotation region 25% further away from the planet and 25% closer to it.

As with method (i) for estimating corotation torques,

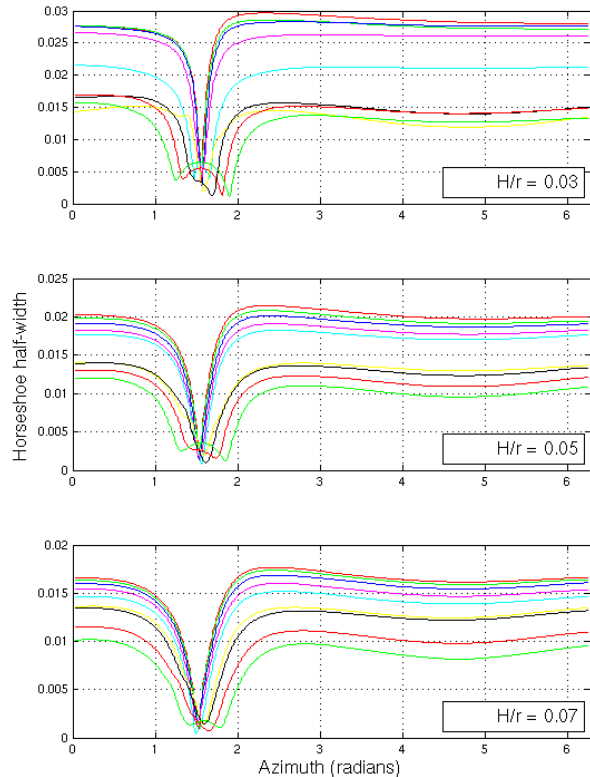


Figure 6. For three different disc aspect ratios, and eccentricities in the range 0 to 0.3, we plot the horseshoe half-width, defined here as half the separation between the inner and outer last circulating streamlines, as a function of azimuth. As the eccentricity increases, the overall horseshoe width decreases and a “double-cusp” reflects the planet’s epicyclic motion for larger values of e . These values were calculated using discs with optimally unsaturated steady-state corotation torques.

this method also suffers from a drawback, which is that high density material that forms close to the planet at apo- and pericentre can enter the defined horseshoe region. Even though these high density features are not related to the horseshoe drag, they nonetheless can contribute to the estimate of the torque using method (ii) because we have no way of excluding them from the torque calculation. In terms of the magnitude of the corotation torque estimate, this method gives a lower value than the other two because of this effect. We note, however, that this method gives a smoothly varying monotonic estimate of the corotation torque as a function of eccentricity, unlike methods (i) and (iii), demonstrating that the steady corotation torque in a viscous disc with cooling really does behave in the expected manner.

3.3 Method (iii): Initial peak of torque time series

This method is the most comparable to that used in previous work (e.g. Paardekooper et al. 2010). We begin by using a Fourier transform filter to remove high frequency oscillations from torque time series obtained from simulations in

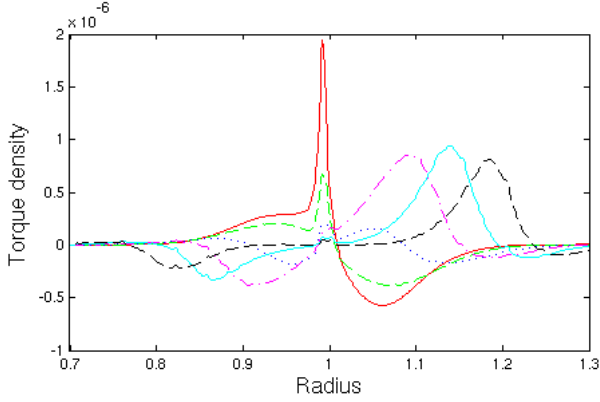


Figure 7. Torque as a function of radius for a disc with $h = 0.07$ and a sustained corotation torque. Eccentricities shown are 0 (red, solid), 0.04 (green, dashed), 0.08 (blue, dotted), 0.12 (magenta, dot-dash), 0.16 (cyan, solid), 0.20 (black, dashed). Note the Lindblad torque reversal for $e > 1.1h$ manifested as the reversal of the sign of the torque contributions from both the inner and outer disc. Also note the clear localisation of the corotation torque to the corotation region.

set A. We then measure the difference between the long-term steady state (Lindblad) torque in these low viscosity adiabatic discs, and the torque value immediately after approximately one horseshoe libration period has elapsed when the surface density perturbations in the horseshoe region have been set up through the advection of entropy and vortensity. This is the moment when the transient corotation torque reaches its maximum positive value, as shown for example by the dashed line in figure 1. Corotation torque estimates obtained using this method are shown in figure 9. As with method (i), this method also has some drawbacks, because the long-term torque that is supposed to represent the Lindblad torque is influenced by the previously described gap and vortex formation.

3.4 A thicker disc: $h = 0.1$

The simulations described above adopted discs with aspect ratios in the range expected for protoplanetary discs. Our results, however, show significant dependence on the disc thickness because of non-linear effects, so we consider a thicker disc model with $h = 0.1$. We have repeated the corotation torque estimates obtained from methods (i), (ii) and (iii) for a broad range of eccentricities, and the corotation torque values are plotted in figure 10. The plots in this figure confirm the general trends noted for the thinner disc models: improvement in the behaviour of torque estimates as one employs thicker disc models; a tendency for method (ii) to produce a low estimate for the corotation torque; and clear decrease in corotation torque as the eccentricity increases.

4 DISCUSSION

In this section, we analyse the fits that predict exponential decay of the corotation torque with increasing eccentricity that we have shown in the figures presented in the previous section, and discuss discrepancies between some of our

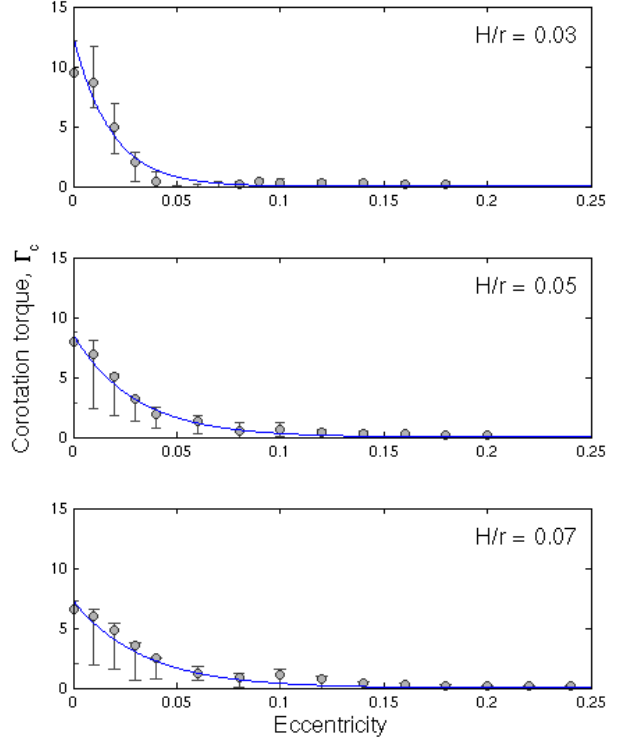


Figure 8. We plot the corotation torque measured by method (ii) by summing the steady-state torque applied to the planet from the material inside last circulating streamlines. Calculations are performed for simulation set B, with a sustained corotation torque. Error-bars are calculated by performing the same calculation with the boundaries moved 25% further away from the planet and 25% closer respectively. Note that this method underestimates the torque compared to the other two. Results are given for three disc aspect ratios and fits are of the form $\Gamma_c = \Gamma_{c,e=0} \exp(-e/e_f)$. Corotation torque is given in units of Γ_0/γ .

simulation results and this trend. We also discuss some limitations of our experimental method, and go on to show how our results are broadly consistent with previous work relating the corotation torque to the horseshoe width.

4.1 Fitting formulae

Before discussing the fitting procedure, we recall that the total corotation torque is given as a sum of the barotropic and entropy-related contributions: $\Gamma_c = \Gamma_{c,\text{baro}} + \Gamma_{c,\text{ent}}$ (Paardekooper et al. 2011). Furthermore, these contributions to the unsaturated horseshoe drag scale with the width of the horseshoe region according to $\Gamma_c \sim x_s^4$. Both $\Gamma_{c,\text{baro}}$ and $\Gamma_{c,\text{ent}}$ depend on the relative time scales associated with horseshoe libration and the viscous/thermal diffusion time scales, as these determine the level of torque saturation. As we have discussed already, the width of the horseshoe region, x_s , depends on the planetary eccentricity, so we might expect the magnitude of the corotation torque for an eccentric planet in a disc with fixed thermal and viscous evolution times to decrease through the x_s^4 dependence, and to also de-

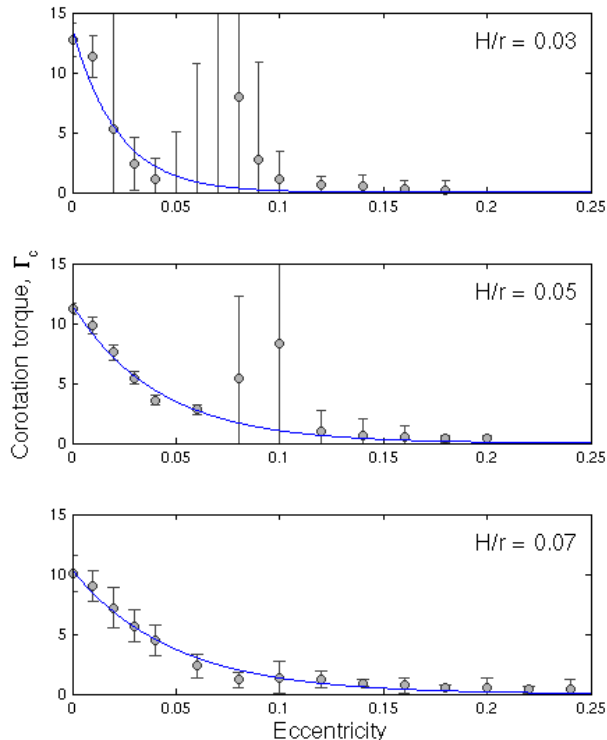


Figure 9. We plot the corotation torque measured by method (iii) described in the text. Error-bars are three times the combined standard deviation of the initial peak and the steady state value. Results are given for three disc aspect ratios $H/r = 0.03, 0.05$ and 0.07 , and fits are of the form $\Gamma_c = \Gamma_{c,e=0} \exp(-e/e_f)$. Corotation torque is given in units of Γ_0/γ .

crease compared to the circular orbit case through changes in the level of torque saturation.

In principle it is possible to disentangle these two effects when fitting the results of the simulations, but this would require a CPU-intensive programme of runs in which the optimal values for the viscosity and thermal relaxation are sought for each value of planet eccentricity. We avoid this complication by fitting a simple function to the simulation results.

Denoting the corotation torque for a zero-eccentricity orbit as $\Gamma_{c,e=0}$, normalised by Γ_0/γ , where we remind the reader that Γ_0 is given by equation 7, we fit the torque as a function of eccentricity using the expression

$$\Gamma_c(e) = \Gamma_{c,e=0} \exp\left(-\frac{e}{e_f}\right). \quad (8)$$

We note that because of the normalisation by Γ_0 , the zero-eccentricity corotation torque is expected to be independent of q and h when in the linear regime. This is because the horseshoe width is expected to scale as $x_s \sim \sqrt{q/h}$, cancelling the $(q/h)^2$ dependence contained in Γ_0 . For larger values of q , or small values of h , however, the width of the corotation torque increases because of its sensitivity to the relative strengths of planet gravity and thermal pressure (Masset et al. 2006; Paardekooper & Papaloizou 2009). This causes $\Gamma_{c,e=0}$ to increase in our simulations as h de-

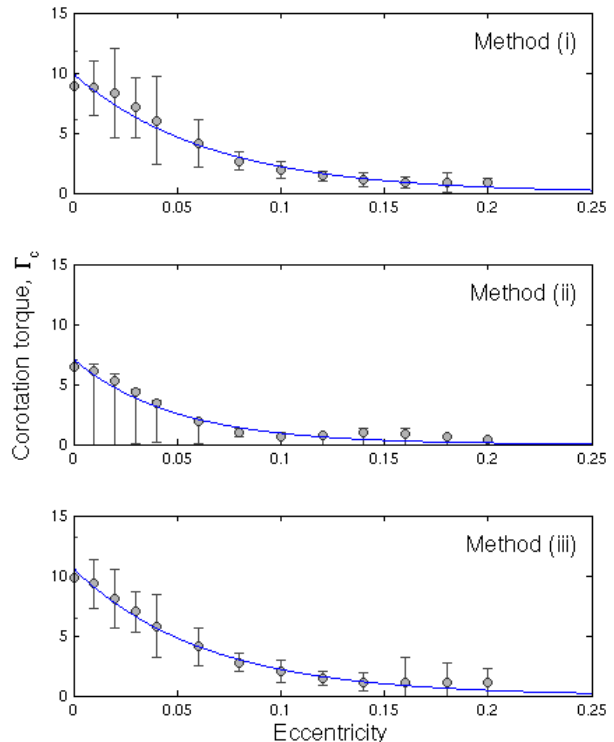


Figure 10. For the disc with the largest aspect ratio, $h = 0.1$, we calculate the corotation torque using the three methods detailed in the test. The fits are of the form $\Gamma_c = \Gamma_{c,e=0} \exp(-e/e_f)$. Corotation torque is given in units of Γ_0/γ .

creases, as shown in figure 11 where we plot $\Gamma_{c,e=0}$ versus h . We note that for $h = 0.05$, our value of $\Gamma_{c,e=0}$ obtained with methods (i) and (iii) agrees well with the canonical value of 11.25 shown in figure 17 of Paardekooper et al. (2010), who also examined this issue. Furthermore, in that paper it was suggested that as q increases or h decreases, it is appropriate to change the value of the coefficient C in the expression

$$\frac{x_s}{r_p} = C \left(\frac{b/h}{0.4}\right)^{1/4} \sqrt{\frac{q}{h}} \quad (9)$$

from $C = 1.1$ in the fully linear regime to 1.3 in the quasi-nonlinear regime to account for this effect in the torque formulae.

We now consider fitting the characteristic e-folding eccentricity, e_f . In figure 12 we plot the best fitting values of e_f obtained using each of the methods (i), (ii) and (iii) as a function of the disc aspect ratio h . Methods (i) and (iii) give very similar values, and method (ii) gives values that are offset slightly but with a similar slope. All methods give an approximately linear relation between e_f and h . The superimposed line in the plot is given by

$$e_f = h/2 + 0.01, \quad (10)$$

Using this relationship, and the one in equation 8, it is possible to obtain the corotation torque attenuation experienced by an eccentric planet.

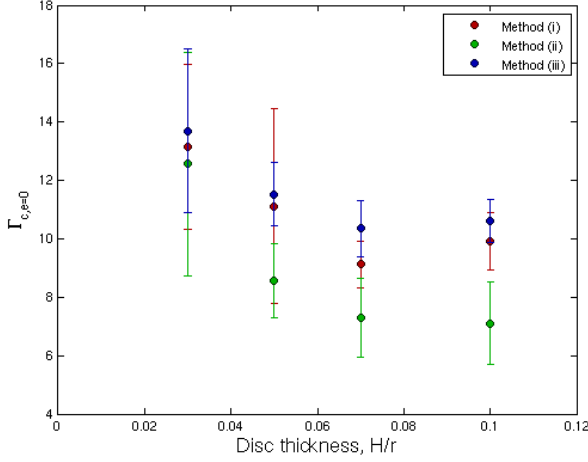


Figure 11. For the twelve simulations plotted as figures 4, 8, 9 and 10, we take the fits of the form $\Gamma_c(e) = \Gamma_{c,e=0} \exp\left(-\frac{e}{e_f}\right)$ and plot $\Gamma_{c,e=0}$ as a function of disc aspect ratio. Error-bars are taken from the 95% confidence intervals of the fits.

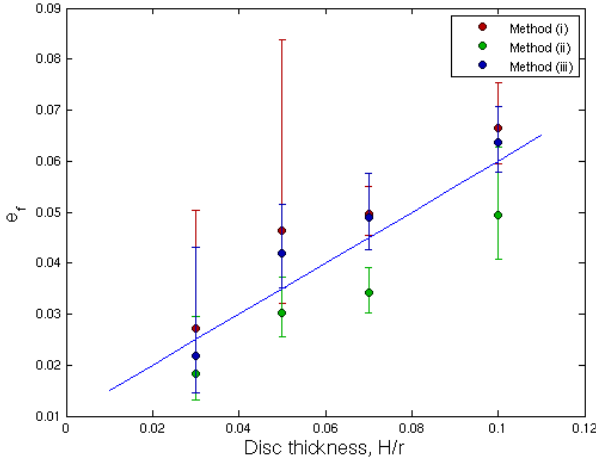


Figure 12. For the twelve simulations plotted as figures 4, 8, 9, 10, we take the fits of the form $\Gamma_c(e) = \Gamma_{c,e=0} \exp\left(-\frac{e}{e_f}\right)$ and plot e_f as a function of disc aspect ratio. Error-bars are taken from the 95% confidence intervals of the fits. We superimpose a simple linear fit of $e_f = h/2 + 0.01$.

4.2 A higher mass planet

So far we have only considered variations in the disc aspect ratio and planet eccentricity, for which the fitting formulae presented in the previous section provide good overall fits to the data, as shown in the figures 4, 8, 9 and 10. We now demonstrate that these fits also give good results when applied to a planet with $10 M_{\oplus}$ instead of $5 M_{\oplus}$. Figure 13 shows the corotation torque estimated using method (iii) from simulations with $h = 0.1$ and a planet with $m_p = 10 M_{\oplus}$. We observe that the fitting formulae given by equations 8 and 10 give very satisfactory results for this case, suggesting that they can be used for a broad range of planet masses, eccentricities and disc aspect ratios. In par-

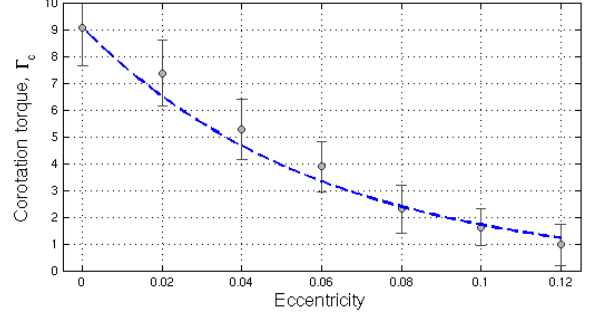


Figure 13. Corotation torque for a $10 M_{\oplus}$ planet embedded in a $h = 0.10$ disc, measuring using our method (iii). Error bars are given to 1σ . We superimpose a fit of the form $\Gamma_c(e) = \Gamma_{c,e=0} \exp(-e/e_f)$, using e_f from equation 10, derived from a study of $5 M_{\oplus}$ planets.

ticular, we note that the characteristic e-folding eccentricity depends only on the disc aspect ratio and not on planet mass, at least for the range of parameters that we have considered.

4.3 Physical interpretation

Material at the edge of the horseshoe region, orbiting at a radial distance of x_s from the planet's location, will have a horseshoe libration time of

$$\tau_{lib} = \frac{8\pi a_p}{3x_s \Omega_p}. \quad (11)$$

As this is much longer than the orbital period of the planet, and its epicyclic motion in the rotating frame, we can say that material in the horseshoe region interacts with the planet on time scales that are long compared to the orbital period. The planet's potential, as experienced by the material librating with respect to it on horseshoe orbits, may therefore appear softened due to its periodic radial excursion from the corotation radius when averaged over one horseshoe libration period. We tentatively suggest that this softening of the potential is responsible for the observed narrowing of the horseshoe width, x_s , as the eccentricity increases. An alternative hypothesis for the observed narrowing of the horseshoe region is that the excursion in azimuth of the planet as it undergoes epicyclic motion causes the horseshoe streamlines that approach the planet most closely to be disrupted. Given that these streamlines are the ones that define the outer edge of the horseshoe region, this would cause the horseshoe region to narrow. We have examined the horseshoe streamlines in some detail for increasing values of the planet eccentricity and can confirm that this is not the case. Instead, we observe that as the eccentricity increases the azimuthal location of the horseshoe u-turns moves away from the planet in a smooth manner.

The interpretation that the corotation torque decreases with increasing eccentricity because of effective gravitational softening leads us to view the eccentricity as the dimensionless length scale associated with epicyclic motion. Consequently, we expect on physical grounds that the e-folding eccentricity, e_f , will depend on a characteristic length scale in the problem. In a real three-dimensional disc there are only two natural length scales that may influence the corotation

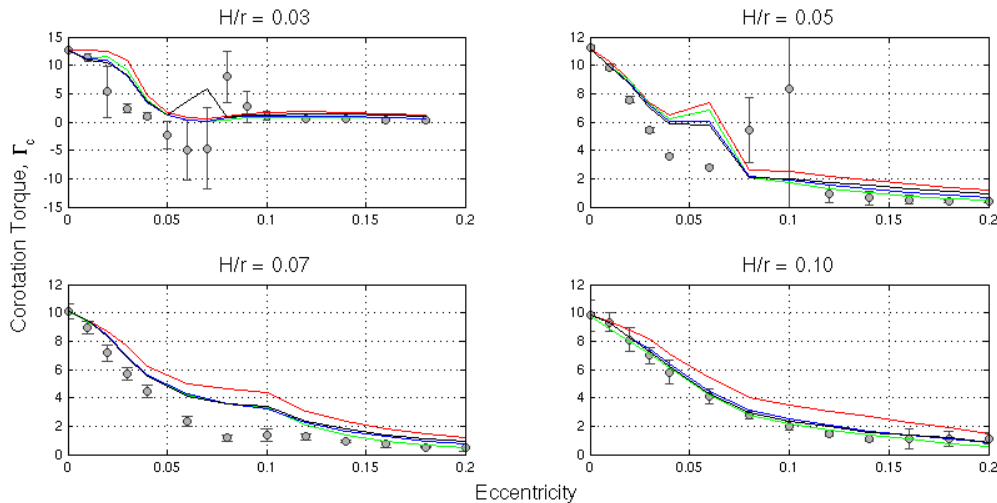


Figure 14. For all our disc aspect ratios we plot corotation torque against eccentricity in units of Γ_0/γ , as measured by method (iii). Error bars are now only one standard deviation. We superimpose lines representing different measures of the horseshoe width. The red line is the width measured at azimuth, $\theta = 0$; the green line corresponds to $\theta = 3\pi/2$; the blue line refers to the horseshoe width for θ just beyond the location of the dip due to the planet’s location; the black line is the maximum value of the horseshoe width.

torque, these being the horseshoe width for a circular orbit, x_s , and the local pressure scale height, h . In earlier work, Hellary & Nelson (2012) suggested that the decrease in the corotation torque with increasing eccentricity observed by Bitsch & Kley (2010) was due to the planet moving outside of the horseshoe region, leading to the assumption that the important parameter in the problem is e/x_s . The simulations of Bitsch & Kley (2010) adopted parameters such that $x_s \sim h$, so determining whether e/x_s or e/h is the important parameter is difficult from their work. Our simulations have been designed to specifically address this question, and show unambiguously that e/h is the important parameter because the e-folding eccentricity is a linear function of the scale height through $e_f = h/2 + 0.01$. Indeed, x_s decreases as h increases due to the pressure in the disc acting as a buffer against the gravitational potential of the planet, so there is no room for doubt from our simulations about whether it is e/h or e/x_s that controls the rate at which the corotation torque decreases as the eccentricity increases. The buffering influence of the pressure explains why e/h determines the magnitude of the corotation torque: the eccentricity of the planet is competing with the pressure in determining the width of the corotation region, so for appreciable changes in x_s to occur it seems that e must be comparable to h .

Our simulations are two-dimensional and require the use of a gravitational softening parameter, b , whose primary role is to allow two-dimensional results to agree with three-dimensional simulations by accounting for missing 3D effects. Normally, b is chosen to be a linear function of H , with values typically being on the order of $0.4H$ as in this work. The introduction of b brings another length scale into the problem that may influence the scaling of the corotation torque with eccentricity. We present a suite of runs in appendix A to examine this, where the scale height remains constant at $h = 0.07$, b/h takes values from 0.2 up to 0.8, and for each value of b/h the eccentricity takes on values between $e = 0$ and $e = 0.12$. We follow the same procedure

described in section 4.1 in obtaining a fit to the corotation torque ($\Gamma_c(e) = \Gamma_{c,e=0} \exp[-e/e_f]$), and examine whether or not e_f can be expressed as a linear function of dimensionless b . Our results demonstrate that this is not the case. At best e_f is a very weak function of b , and is consistent with our original fit $e_f = h/2 + 0.01$. This result demonstrates that it is the scale height, h , and not the softening, b , that determines the behaviour of the corotation torque as e increases in our simulations. Although the reason for this is not entirely clear, we suggest that the primary reason is that the width of the horseshoe region x_s is being controlled primarily by the scale height, h , rather than the softening parameter, b , in most of our runs, so that the softening effect introduced by increasing the eccentricity is competing with h rather than b . Some support for this interpretation is provided by the fact that x_s has a stronger functional dependence on the scale height, h , than on the softening, b .

If this interpretation is true then it implies that there is a range of values of b for which the softening plays the most important role in controlling x_s , and for that range of values we would expect e/b to control the rate at which the corotation torque decreases as e increases. The values of b for which this is true are likely to be significantly larger than $0.4H$, meaning that this parameter regime lies outside of the range of models that closely mimic the behaviour expected for 3D simulations that require $b \sim 0.4H$.

We note that the previously mentioned gravitational softening due to the planet’s epicyclic motion can be observed to operate in our simulations by comparing runs on a case by case basis. For an eccentric orbit the apparent softening length is $b_*^2 = b^2 + e^2 a^2$. We therefore expect that, for example, a $5M_\oplus$ planet on a circular orbit in a disc with $h = 0.07$ with $b/h = 0.8$ will exhibit the same corotation torque as a run with $b/h = 0.4$ and $e = 0.0485$, and this is indeed found to be the case in our runs within the margin of error involved in measuring corotation torques. This

adds further weight to the physical interpretation described above.

Finally, we now discuss how consistent our results are with the interpretation that the corotation torque decreases because the horseshoe width narrows with increasing eccentricity. As mentioned already in the analysis by Ward (1991), and later work by Masset (2001) and Paardekooper et al. (2010), the width of the corotation region is related to the corotation torque by the scaling:

$$\Gamma_c \sim x_s^4. \quad (12)$$

In figure 14, we attempt to fit just such a scaling to our torque measurements obtained using method (iii), normalised to match the measured torque at zero-eccentricity. Although the overall scaling, covering the full range of eccentricity values considered, is reasonably well captured by the curves, it is clear that the corotation torques in the simulations fall off faster than predicted by the x_s^4 scaling. One possible explanation for this is that the narrowing of the horseshoe region causes the thermal relaxation time and viscosity in the simulations to be no longer optimal for unsaturating the torque, leading to a further reduction in its value beyond the fall off predicted by the x_s^4 scaling.

4.4 Corotation torque set-up timescale

A planet on a circular orbit migrating because of tidal interaction with the disc will retain the material in the horseshoe region as it migrates. Consequently the corotation torque will evolve gradually as the semi-major axis changes. A planet that experiences a very rapid change in its position in the disc, however, due to planet-planet scattering, will set up a new corotation region with material undergoing horseshoe libration. The scattering will likely leave the planet in an eccentric orbit initially when it lands at the new semi-major axis, so the growth of the new corotation torque will occur on the time scale for eccentricity damping, followed by the libration time scale given by equation 11 as the planet tends toward a circular orbit. In general, standard type I migration time scales are on the order of 10^4 orbits for $1 M_\oplus$ planets, and $\sim 10^3$ orbits for $10 M_\oplus$ bodies (e.g. Tanaka et al. 2002). The eccentricity damping time scale is typically a factor $\sim (H/r)^2$ shorter than the migration time (Tanaka & Ward 2004), bringing it close to the time scales for horseshoe libration for low mass planets. As such, the damping of eccentricity and growth of the corotation torque will occur on similar time scales. In principle, these are issues that should be accounted for in N-body simulations of planetary formation that include prescriptions for corotation torques, if planet-planet scattering plays an important role.

5 CONCLUSION

In this paper we have presented a suite of simulations that were designed to examine how the steady disc-induced corotation torque varies as a function of planet orbital eccentricity for low mass planets embedded in protoplanetary discs. We considered disc models with four different aspect ratios, and used three different methods to estimate the corotation torque. In agreement with previous work (Bitsch & Kley

2010), we find that the corotation torque decreases as the orbital eccentricity increases. We provide an analytical fit to the numerically-obtained corotation torques as a function of eccentricity, and find that they are well-fitted by a simple exponential decay with e-folding eccentricity that scales linearly with the disc aspect ratio.

Through inspection of time-averaged fluid streamlines we find that the fluid in the corotation region continues to undergo horseshoe orbits when the eccentricity is non-zero. As the eccentricity increases we find that the horseshoe region narrows, and we suggest that this is the major reason why the corotation torque decreases with increasing eccentricity, since the non-linear horseshoe drag, Γ_c , is known to scale as $\Gamma_c \sim x_s^4$. When plotting the measured values of Γ_c against the measured values of x_s we find that the corotation torques from the simulations drop off more rapidly than suggested by the x_s^4 scaling. We tentatively suggest that the changing width of the horseshoe region causes the adopted values of thermal relaxation time and viscosity in the simulations to become suboptimal for fully unsaturating the corotation torque, causing the torque to be smaller than predicted by the x_s^4 scaling.

While previous work (e.g. Hellary & Nelson 2012) has made use of a simple model of corotation torque as a function of eccentricity, wherein the parameter governing the torque attenuation is e/x_s , we have shown instead that the torque decays as e/e_f , where e_f can be modelled as a linear function of the disc aspect ratio. This latter scaling produces a less severe drop-off in the magnitude of the corotation torque with eccentricity, as the scale height is generally larger than the horseshoe width for low mass embedded planets. The fitting formula we have provided should therefore provide a useful addition to N-body models of planet formation that implement type I migration prescriptions including corotation torques, especially if planet-planet scattering events are important.

Our results have implications for the notion of ‘‘zero torque radii’’ occurring in discs at locations where the (outward) corotation torque balances the (inward) Lindblad torque. Such locations may be important during planetary formation by acting as ‘traps’ where planetary building blocks may congregate, enhancing accretion. While the locations of these zero torque radii depend on the properties of the local disc sufficiently optimising the corotation torque, we have shown that a relatively modest planetary eccentricity can have an effect on the torque experienced by the planet, moving the location of zero torque radii, or even removing them entirely if the eccentricities become large enough, resulting in a qualitative effect on planetary migration and formation. One particular scenario where this may be important is in the formation of circumbinary planets, where the disturbing influence of the central binary may excite significant eccentricities, as considered recently by Pierens & Nelson (2013) in application to the Kepler-16, 34 and 35 systems.

Furthermore, as eccentricities are often excited by planetary bodies in mean motion resonance, our work has implications for pairs of planets being able to remain in resonance after having their eccentricities excited, and therefore on the subsequent evolution of such a system. For example, a pair of planets may migrate convergently into resonance, because of the influence of corotation torques, excite their mutual

eccentricities, and then migrate divergently such that the resonance is not maintained. Subsequent damping of the eccentricity will then cause this process to repeat, keeping the system near to, but not actually in resonance. Such a mode of evolution could potentially explain the compact systems of low-mass planets discovered by the Kepler mission (e.g. Kepler-11 (Lissauer et al. 2011)) which are close to, but not in resonance.

This work has been limited in using a simple thermal model in a 2D disc. In future work we plan to revisit some of the issues raised in the paper using 3D models of discs with radiative transfer.

ACKNOWLEDGEMENTS

SMF acknowledges the support of an STFC PhD studentship. The simulations presented in this paper were performed on the QMUL HPC facility purchased under the SRIF initiatives.

REFERENCES

- Baruteau C., Masset F., 2008, *The Astrophysical Journal*, 672, 1054
- Bitsch B., Kley W., 2010, *Astronomy & Astrophysics*, 523
- Borucki W. J., Agol E., Fressin F., Kaltenegger L., Rowe J., Isaacson H., Fischer D., Batalha N., Lissauer J. J., Marcy G. W., et al., 2013, *Science*, 340, 587
- Cresswell P., Nelson R., 2006, *Astronomy and Astrophysics*, 450, 833
- Crida A., Morbidelli A., Masset F., 2006, *Icarus*, 181, 587
- Endl M., Robertson P., Cochran W. D., MacQueen P. J., Brugamyer E. J., Caldwell C., Wittenmyer R. A., Barnes S. I., Gullikson K., 2012, *The Astrophysical Journal*, 759, 19
- Fabrycky D. C., Ford E. B., Steffen J. H., Rowe J. F., Carter J. A., Moorhead A. V., Batalha N. M., Borucki W. J., Bryson S., Buchhave L. A., et al., 2012, *The Astrophysical Journal*, 750, 114
- Gautier III T. N., Charbonneau D., Rowe J. F., Marcy G. W., Isaacson H., Torres G., Fressin F., Rogers L. A., Désert J.-M., Buchhave L. A., et al., 2012, *The Astrophysical Journal*, 749, 15
- Goldreich P., Tremaine S., 1980, *ApJ*, 241, 425
- Hayashi C., 1981, *Progress of Theoretical Physics Supplement*, 70, 35
- Hellary P., Nelson R. P., 2012, *Monthly Notices of the Royal Astronomical Society*, 419, 2737
- Kley W., Nelson R., 2012, *Annual Review of Astronomy and Astrophysics*, 50, 211
- Lin D. N. C., Papaloizou J. C. B., 1993, in Levy E. H., Lunine J. I., eds, *Protostars and Planets III On the tidal interaction between protostellar disks and companions*. pp 749–835
- Lissauer J. J., Fabrycky D. C., Ford E. B., Borucki W. J., Fressin F., Marcy G. W., Orosz J. A., Rowe J. F., Torres G., Welsh W. F., Batalha N. M., Bryson S. T., Buchhave L. A., Caldwell D. A., Carter J. A., 2011, *Nature*, 470, 53
- Lissauer J. J., Fabrycky D. C., Ford E. B., Borucki W. J., Fressin F., Marcy G. W., Orosz J. A., Rowe J. F., Torres G., Welsh W. F., et al., 2011, *Nature*, 470, 53
- Lissauer J. J., Marcy G. W., Rowe J. F., Bryson S. T., Adams E., Buchhave L. A., Ciardi D. R., Cochran W. D., Fabrycky D. C., Ford E. B., et al., 2012, *The Astrophysical Journal*, 750, 112
- Lovis C., Ségransan D., Mayor M., Udry S., Benz W., Bertaux J.-L., Bouchy F., Correia A., Laskar J., Lo Curto G., et al., 2011, *Astronomy & Astrophysics*, 528
- Masset F. S., 2001, *ApJ*, 558, 453
- Masset F. S., Casoli J., 2010, *ApJ*, 723, 1393
- Masset F. S., D’Angelo G., Kley W., 2006, *ApJ*, 652, 730
- Masset F. S., Morbidelli A., Crida A., Ferreira J., 2006, *ApJ*, 642, 478
- McNeil D. S., Nelson R. P., 2010, *MNRAS*, 401, 1691
- Muto T., Suzuki T., Inutsuka S., 2010, *The Astrophysical Journal*, 724, 448
- Paardekooper S., Baruteau C., Crida A., Kley W., 2010, *Monthly Notices of the Royal Astronomical Society*, 401, 1950
- Paardekooper S., Baruteau C., Kley W., 2011, *Monthly Notices of the Royal Astronomical Society*, 410, 293
- Paardekooper S., Mellema G., 2006, *Astronomy and Astrophysics*, 459, 17
- Paardekooper S., Papaloizou J., 2008, *Astronomy and Astrophysics*, 485, 877
- Paardekooper S.-J., Papaloizou J., 2009, *Monthly Notices of the Royal Astronomical Society*, 394, 2297
- Papaloizou J., Larwood J., 2002, *Monthly Notices of the Royal Astronomical Society*, 315, 823
- Pierens A., Nelson R. P., 2013, *ArXiv e-prints*
- Rafikov R. R., 2002, *ApJ*, 572, 566
- S. Udry X. Bonfils X. Delfosse T. Forveille M. Mayor C. Perrier F. Bouchy C. Lovis F. Pepe D. Queloz J.-L. Bertaux 2007, *A&A*, 469, L43
- Stone J. M., Norman M. L., 1992, *ApJS*, 80, 753
- Tanaka H., Takeuchi T., Ward W. R., 2002, *ApJ*, 565, 1257
- Tanaka H., Ward W. R., 2004, *ApJ*, 602, 388
- Val-Borro D., Edgar R., Artymowicz P., Cielieglag P., Cresswell P., D’Angelo G., Delgado-Donate E., Dirksen G., Fromang S., Gawryszczak A., et al., 2006, *Monthly Notices of the Royal Astronomical Society*, 370, 529
- Ward W. R., 1991, in *Lunar and Planetary Institute Science Conference Abstracts Vol. 22 of Lunar and Planetary Institute Science Conference Abstracts, Horsehoe Orbit Drag*. p. 1463
- Ward W. R., 1997, *Icarus*, 126, 261
- Weidenschilling S. J., 1977, *APSS*, 51, 153
- Wright J. T., Fakhouri O., Marcy G. W., Han E., Feng Y., Johnson J. A., Howard A. W., Fischer D. A., Valenti J. A., Anderson J., Piskunov N., 2011, *Publications of the Astronomical Society of the Pacific*, 123, pp. 412
- Ziegler U., 1998, *Computer physics communications*, 109, 111

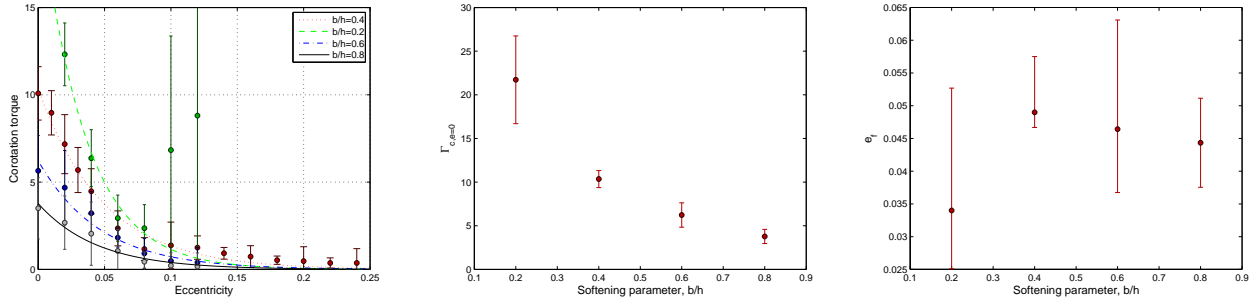


Figure A1. Left panel: the corotation torque on a $5M_{\oplus}$ planet in units of Γ_0/γ obtained using method (iii). We superimpose fits of the form $\Gamma_c = \Gamma_{c,e=0} \exp(-e/e_f)$ over these data. Middle panel: We show the parameter $\Gamma_{c,e=0}$ from the fits shown in the left panel, as a function of softening, b/h . Right panel: We show the parameter e_f from the fits shown in the left panel, as a function of the softening, b/h .

APPENDIX A: DEPENDENCE ON THE SOFTENING PARAMETER, b/h

In order for 2D hydrodynamic simulations to produce results comparable to 3D ones, it is necessary to introduce a gravitational softening parameter, b , to compensate for absent 3D effects. This parameter is taken to be a linear function of the local height of the disc, typically on the order of $0.4h$ as in this paper.

Given our tentative physical explanation of why the corotation torque decreases with eccentricity given in Sect. 4.3, based on the idea that the epicyclic motion of the planet induces an effective softening of the planet potential, here we examine whether or not the softening parameter, b , or the scale height, h , are most important for setting the scaling of e_f , the e-folding eccentricity used in our analytical fits. To this end, we ran a series of simulations of a $5M_{\oplus}$ planet embedded in a $h = 0.07$ disc, with values of b/h between 0.2 and 0.8. We again perform fits of the form $\Gamma_c = \Gamma_{c,e=0} \exp(-e/e_f)$, and show these superimposed on the data in the left panel of figure A1. We note that using a small value of $b/h = 0.2$ can also lead to non-linear restructuring of the disk, similar to described in Sect. 3.1, explaining the outlying points at eccentricity values $e = 0.1$ and 0.12 .

The values we obtain for the parameter $\Gamma_{c,e=0}$ are shown in the middle panel of figure A1. We note that in the circular orbit case, we expect the corotation torque to scale as x_s^4 , and therefore as $\frac{1}{b/h}$, and our data are consistent with this. The e-folding eccentricity values, e_f , are shown in the right panel of figure A1 as a function of b/h . We observe no obvious trend, and the best fitting values appear to be independent of b/h . We note, however, that using equation 10 ($e_f = h/2 + 0.01$) yields a value $e_f = 0.045$, which is consistent with the results shown in the right panel of figure A1.

We conclude that the key physical quantity that determines the behaviour of e_f is the disc scale height h . The softening parameter, b , plays the important role of allowing 2D simulations to produce results that are consistent with 3D simulations, but does not play an important role in determining how the corotation torque scales with orbital eccentricity.

This paper has been typeset from a \LaTeX file prepared by the author.